

Excitons in Bulk and Layered Chromium Tri-Halides: From Frenkel to the Wannier-Mott Limit

Swagata Acharya,¹ Dimitar Pashov,² Alexander N. Rudenko,¹ Malte Rösner,¹ Mark van Schilfhaarde,^{3,2} and Mikhail I. Katsnelson¹

¹*Institute for Molecules and Materials, Radboud University, NL-6525 AJ Nijmegen, The Netherlands**
²*King's College London, Theory and Simulation of Condensed Matter, The Strand, WC2R 2LS London, UK*
³*National Renewable Energy Laboratory, Golden, CO 80401, USA*

Excitons with large binding energies $\sim 2-3$ eV in CrX_3 are historically characterized as being localized (Frenkel) excitons that emerge from the atomic $d-d$ transitions between the $\text{Cr-}3d-t_{2g}$ and e_g orbitals. The argument has gathered strength in recent years as the excitons in recently made monolayers are found at almost the same energies as the bulk. The Laporte rule, which restricts such parity forbidden atomic transitions, can relax if, at least, one element is present: spin-orbit coupling, odd-parity phonons or Jahn-Teller distortion. While what can be classified as a purely Frenkel exciton is a matter of definition, we show using an advanced first principles parameter-free approach that these excitons in CrX_3 , in both its bulk and monolayer variants, have band-origin and do not require the relaxation of Laporte rule as a fundamental principle. We show that, the character of these excitons is mostly determined by the $\text{Cr-}d$ orbital manifold, nevertheless, they appear only as a consequence of $\text{X-}p$ states hybridizing with the $\text{Cr-}d$. The hybridization enhances as the halogen atom becomes heavier, bringing the $\text{X-}p$ states closer to the $\text{Cr-}d$ states in the sequence $\text{Cl} \rightarrow \text{Br} \rightarrow \text{I}$, with an attendant increase in exciton intensity and decrease in binding energy. By applying a range of different kinds of perturbations, we show that, moderate changes to the two-particle Hamiltonian that essentially modifies the $\text{Cr-}d\text{-X-}p$ hybridization, can alter both the intensities and positions of the exciton peaks. A detailed analysis of several deep lying excitons, with and without strain, reveals that the exciton is most Frenkel like in CrCl_3 and acquires mixed Frenkel-Wannier character in CrI_3 .

INTRODUCTION

Excitons are charge-neutral excitations, and can be well approximated by the eigenstates of a two-particle Hamiltonian. An electron-hole pair can form an excitonic bound state as the Coulomb interaction becomes strong. These two-particle bound states can form deep inside one-particle electronic band gap in insulators. Usually in systems where the valence and conduction states are mostly dominated by s and p electrons the Coulomb interaction is strongly screened and the excitons become weakly bound. Such excitons are referred to as Mott-Wannier excitons [1] due to their delocalized nature in real space with diameters up to few nanometres. These excitons are heavily studied in the literature and usually their binding energies range between tens of meV to 500 meV [2, 3]. The excitons observed in transition metal dichalcogenides [2, 3], LiF [4] are prototypical example of Wannier-Mott excitons. Only the bottom of the conduction band and the top of the valence band take part in formation of these excitons. Nevertheless, as systems become more strongly correlated, for example, in systems with low-energy flat d -states, the Coulomb interaction between electron and hole increases and they can have large binding energies with a diameter approximately that of an atom in an extreme case. Such strongly localized excitons can have binding energies ~ 1 eV or more and they are referred to as Frenkel excitons [5–7]. Such excitons are heavily studied in molecular systems [8–10] that are far from the band-limit. In a crystalline environment where a band picture is applicable, an entire range of bands [4] that contain character of the orbital where the exciton predominantly resides can contribute to their formation, in strong contrast to the Wannier-Mott excitons.

Recent observations of excitons with high binding energies in two-dimensional ferromagnetic monolayers of CrX_3 [11, 12] have rekindled the investigation of Frenkel excitons in real materials. In a purely atomic picture, the low energy manifold of these systems are determined by the $\text{Cr-}3d t_{2g\uparrow}$ valence orbitals that contributes to magnetic moment of $3 \mu_B/\text{Cr}$ atom and the $\text{Cr-}3d e_{g\uparrow}$ conduction orbitals. In a series of recent experimental studies that perform controlled photoluminescence and other optical measurements on these 2D magnets, excitons are observed at ~ 1 eV [11, 12] while the electronic band gaps of these systems are in the range of ~ 3 -5 eV. These materials are, however, not new and their bulk variants had been studied for long with the earliest studies dating back more than half a century [13–17]. To realise these magnets in their 2D variant is very recent as ferromagnetism (FM) in a monolayer CrI_3 was first reported in 2017 [18, 19], which was followed by observation of FM in CrBr_3 [11, 20], CrCl_3 [21] and many other compounds [22–26]. Bulk and layered variants of the same compound do have different electronic band gaps due to differences in the screening environment originating from their effective dimensionality. Going from bulk to monolayer the electronic screening reduces significantly, leading to a screened Coulomb exchange which is larger than the bulk. Nevertheless, the observation of the same deep lying excitons at almost the same energies both in bulk and monolayer (ml-) CrX_3 is intriguing and suggests that these excitons are Frenkel-like and, could probably be, even the extreme limit of that where they emerge purely from the atomic d - d transitions [12].

In a recent work [27] we showed that both the electronic band gaps and the halogen components in the valence band manifold changes significantly in ml- CrX_3 depending on the nature of the ligand (X) atom. There is significant hybridization of the $\text{Cr-}3d$ states with the X - p states and the degree of hybridization increases significantly in the sequence $\text{Cl} \rightarrow \text{Br} \rightarrow \text{I}$. In this work we show that this hybridization fully controls the exciton intensity, and also to some extent its position.

theory	Monolayer bandgap E_g (eV)			Bulk bandgap E_g (eV)		
	CrCl_3	CrBr_3	CrI_3	CrCl_3	CrBr_3	CrI_3
DFT	1.51	1.30	1.06	1.38	1.21	0.9
QSGW	6.87	5.73	3.25	5.4	4.38	3.0
$\widehat{\text{QSGW}}$	5.55	4.65	2.9	4.4	3.5	2.5
G_0W_0	5.47 [28]	4.45 [28], 3.8 [29]	2.76 [28]			

TABLE I. One particle electronic band gap E_g at different levels of theory (with spin-orbit coupling). The gap increases from LDA to QSGW level. When when ladder diagrams are added two-particle interactions via a BSE, $W \rightarrow \widehat{W}$ and screening is increased. This reduces the QSGW bandgap by ~ 20 -25%. Also E_g reduces in bulk compared to their monolayer variants by $\sim 20\%$. The last line notes E_g values as reported from LDA based single shot G_0W_0 calculations performed by different groups.

We employ our advanced many-body perturbative Green’s function based approach and show how in these materials excitons with high binding energies are sensitive to fine details of the two-particle Hamiltonian. Following our earlier work [27] we employ three different levels of theory: the local-density approximation (LDA), quasiparticle self-consistent GW theory [30–32] (QSGW), which, in contrast to conventional GW , modifies the charge density and is determined by a variational principle [33], and finally an extension $\widehat{\text{QSGW}}$ of QSGW, where the polarizability needed to construct W is computed including vertex corrections (ladder diagrams) by solving a Bethe-Salpeter equation

(BSE) for the two-particle Hamiltonian [34]. The electron-hole two-particle correlations are incorporated within this self-consistent ladder-BSE $QSG\widehat{W}$ implementation [34, 35] within the Tamm-Dancoff approximation [36, 37]. As the present work is a study of excitons, we consider here only $QSG\widehat{W}$ calculations. A crucial difference in our implementation of $QSG\widehat{W}$ from most other implementations of BSE is that the calculations are self-consistent in both self energy Σ and the charge density [27, 38]. The effective interaction W is calculated with ladder-BSE corrections and the self energy, using a static vertex in the BSE. G , Σ and W are updated iteratively until all of them converge. Thus, in contrast to most recent GW studies [28, 29] our calculations are completely parameter free and have no starting point bias. In each cycle, the RPA polarizability is made anew, which determines the RPA \widehat{W} . In each cycle the four-point polarizability is recomputed from the (newly updated) static part of W , to update \widehat{W} . Moreover, we checked the convergence in the $QSG\widehat{W}$ band gap [27] and exciton positions by increasing the size of the two-particle Hamiltonian. We increase the number of valence (v) and conduction (c) states and observe that for all materials the $QSG\widehat{W}$ band gap stops changing once 24 valence and 14 conduction states are included in the two-particle Hamiltonian. This stands in stark contrast to the weakly bound case. It reflects the atomic molecular-like picture where any state with significant orbital character participating in the exciton (Cr-3d or X-p) modify it, not just the band edge states as in the Wannier picture. This allows us the flexibility to pin down the orbital characters that determine the position and intensities of the excitons.

RESULTS AND DISCUSSION

Within $QSG\widehat{W}$, the Coulomb interaction W softens in comparison to $QSGW$, since the screening is enhanced by the electron-hole attraction, as captured by the ladder diagrams. The electronic band gap reduces roughly by 20-25% within $QSG\widehat{W}$ compared to $QSGW$ for all materials both in their bulk and monolayer variants (see Table I). We compute the macroscopic dielectric response $\text{Im}\epsilon_{xx}$ with the perturbing electric field applied along the (100) direction of the material, with the $QSG\widehat{W}$ electronic one-particle eigenfunctions assuming the optical vertex $\Gamma=I$ (identity matrix) and also using the explicitly computed Γ . The excitons inside the one-particle band gap ($E \leq E_g$) can only be present in the second case, and not in the first case where the optical transitions can only occur at or beyond the one-particle band gap ($E \geq E_g$).

We observe that Γ induces dramatic optical spectral weight transfer and series of excitons emerge inside the one-particle band gap $\leq E_g$ in Fig. 1. The optical weight transfers the most for X=Cl and the least for X=I. A series of exciton peaks can be observed in all cases inside the gap. When we zoom into the low energy (0 – 2 eV) part of the optical spectra we observe two deepest lying excitons ex_1 and ex_2 (see Fig. 2) that are robust across all cases and also for both bulk and monolayer variants of CrX_3 . We observe a weak redshift of ~ 0.2 eV of these exciton peaks as the electronic screening reduces going from bulk to monolayer. From the deepest lying exciton ex_1 position E_{ex} and the electronic band gap E_g at the $QSG\widehat{W}$ level, we can compute the highest exciton binding energies as $E_b = E_g - E_{ex}$. E_b enhances significantly in ml compared to the bulk, since lesser screening implies stronger exciton binding in ml. Note, although apparently E_{ex} remains invariant in bulk and ml, both E_g and E_b enhances in ml compared to bulk.

theory	Monolayer E_b (eV)			Bulk E_b (eV)		
	CrCl ₃	CrBr ₃	CrI ₃	CrCl ₃	CrBr ₃	CrI ₃
ex_1	4.75, 2.62 [28]	3.85, 2.05 [28], 2.3 [29]	1.95, 1.06 [28]	3.35	2.5	1.3
ex_2	3.9	3.1	1.35	2.5	1.75	0.7
ex_3	2.3	2.05	0.9	1.1	0.9	0.4

TABLE II. Exciton binding energies E_b for three deepest lying excitons in all cases as computed from the difference between the one particle electronic band gap E_g and position of the exciton peaks E_{ex} . We note the E_b values as reported from LDA based single shot G_0W_0+BSE calculations for dielectric response performed by different groups. In the supplemental material we discuss the possible reasons for their differences with our estimations.

In bulk, these two exciton peaks ($ex_{1,2}$) are experimentally well established in $CrCl_3$ and $CrBr_3$ from a series of works [13–17] performed between 1960’s and 1980’s. In a recent work [39] on $CrCl_{3-x}Br_x$ the same peaks are observed again and also going from $x=3$ to $x=0$ a weak blueshift in the peak positions can be noticed. Within our parameter free approach we can reproduce the two-peaks in both $X=Cl$ and Br and also their relative spacing and intensities agree almost perfectly (see Fig. 3). Some of the crucial features like weak blue shifting of the exciton peaks and change in their relative spacing in $CrCl_3$ compared to $CrBr_3$ are also reproduced in our calculations. However, these two peaks in our calculations are ~ 0.5 eV too deep compared to the experimental findings. The position of these excitons change and they become systematically red-shifted as more screening channels are included in the two-particle

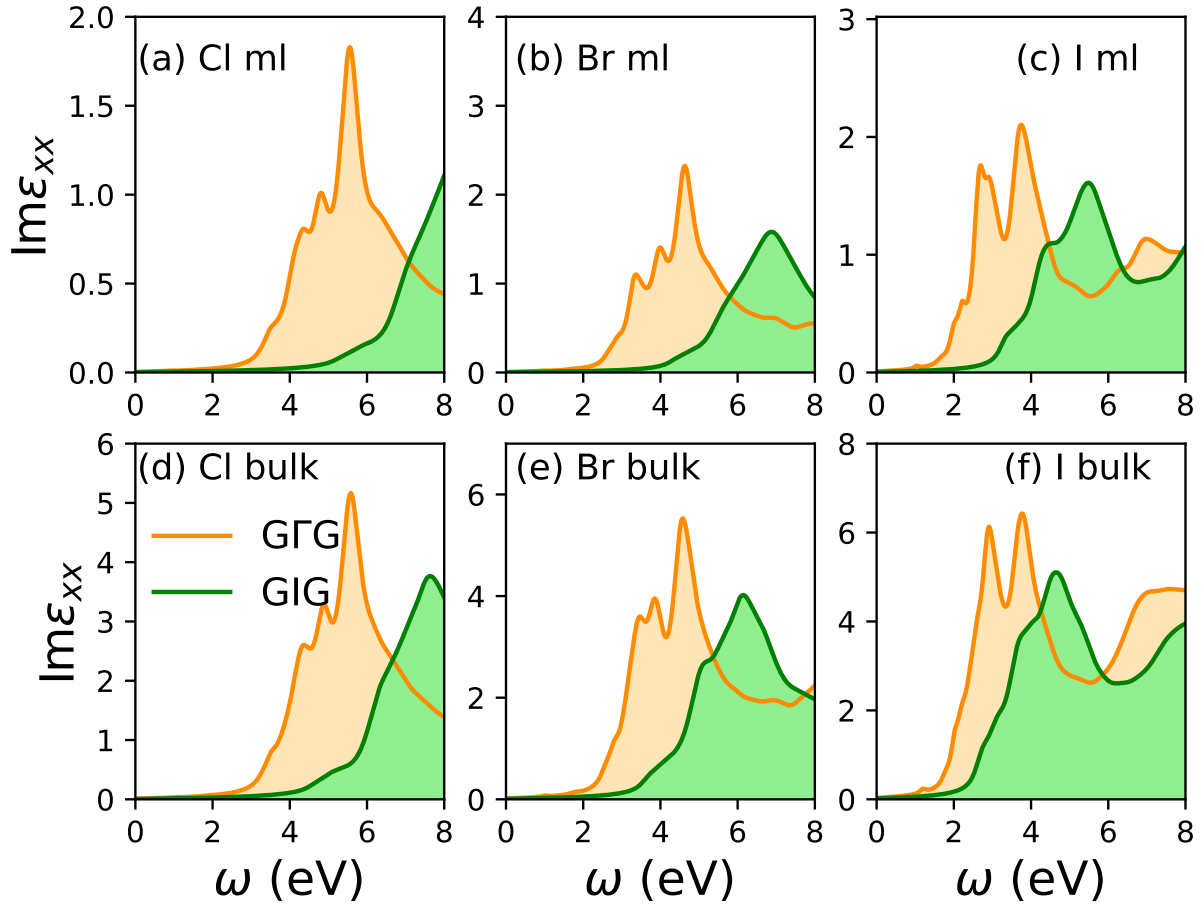


FIG. 1. CrX_3 : Imaginary part of macroscopic dielectric response $\text{Im}\epsilon_{xx}$ with the perturbing electric field applied along the (100) direction of the material, for free standing monolayers (ml) of CrX_3 with (a) $X = \text{Cl}$, (b) $X = \text{Br}$, (c) $X = \text{I}$ and bulk CrX_3 with (d) $X = \text{Cl}$, (e) $X = \text{Br}$ and (f) $X = \text{I}$. The orange color stand for $\widehat{\text{QSGW}}$ vertex Γ corrected optical response, while the green color stands for the vertex replaced by an identity matrix I effectively making it a RPA optical response with $\widehat{\text{QSGW}}$ one-particle eigenfunctions. Energy-dependent optical broadening that linearly varies from 2 milli-Hartree at $\omega = 0$ and 50 milli-Hartree at $\omega = 13.6$ eV is used.

Hamiltonian we solve using $\widehat{\text{QSGW}}$. As we show in the Supplemental material the two peaks already form when the two-particle Hamiltonian contains the minimal 6 valence bands (v) and 4 conduction bands (c), which are mostly of $\text{Cr-}d t_{2g\uparrow}$ character and $\text{Cr-}d e_{g\uparrow}$ character. So these exciton peaks are triplet in nature and emerge from the $3d t_{2g-eg}$ transitions within the bands of mostly Cr character. They red-shift in tandem as two-particle Hamiltonian includes more bands.

In a recent photoluminescence (PL) study on ml- CrBr_3 by Zhang *et al.* [11], the authors observe a peak at 1.35 eV. They also observe that the PL peak energy is almost invariant of thickness of the sample (thickness ranging between 6 and 73 nm), which suggests a localized transition. Based on that they argue that this transition is consistent with an atomic $d-d$ transition. They further argue that that since the Laporte rule prohibits such transition based on symmetry considerations, to relax the rule symmetry breaking must be introduced via at least one mechanism, such as spin-orbit coupling, Jahn-Teller distortion and formation of odd-parity phonons [12] as we noted in the introduction. They observe a broad PL linewidth and argue that it serves as the evidence for the strong vibronic coupling, resulting in photon sidebands. They also note that the absorption peak that Dhillon *et al.* [13] observed at 1.67 eV in their work from 1966 in bulk CrBr_3 is fundamentally the same peak Zhang *et al.* [11] observes at 1.35 eV in ml- CrBr_3 , which is assigned to the absorption to the 4T_2 state at 1.5 K. They argue, further, that the Stokes shift of 320 meV,

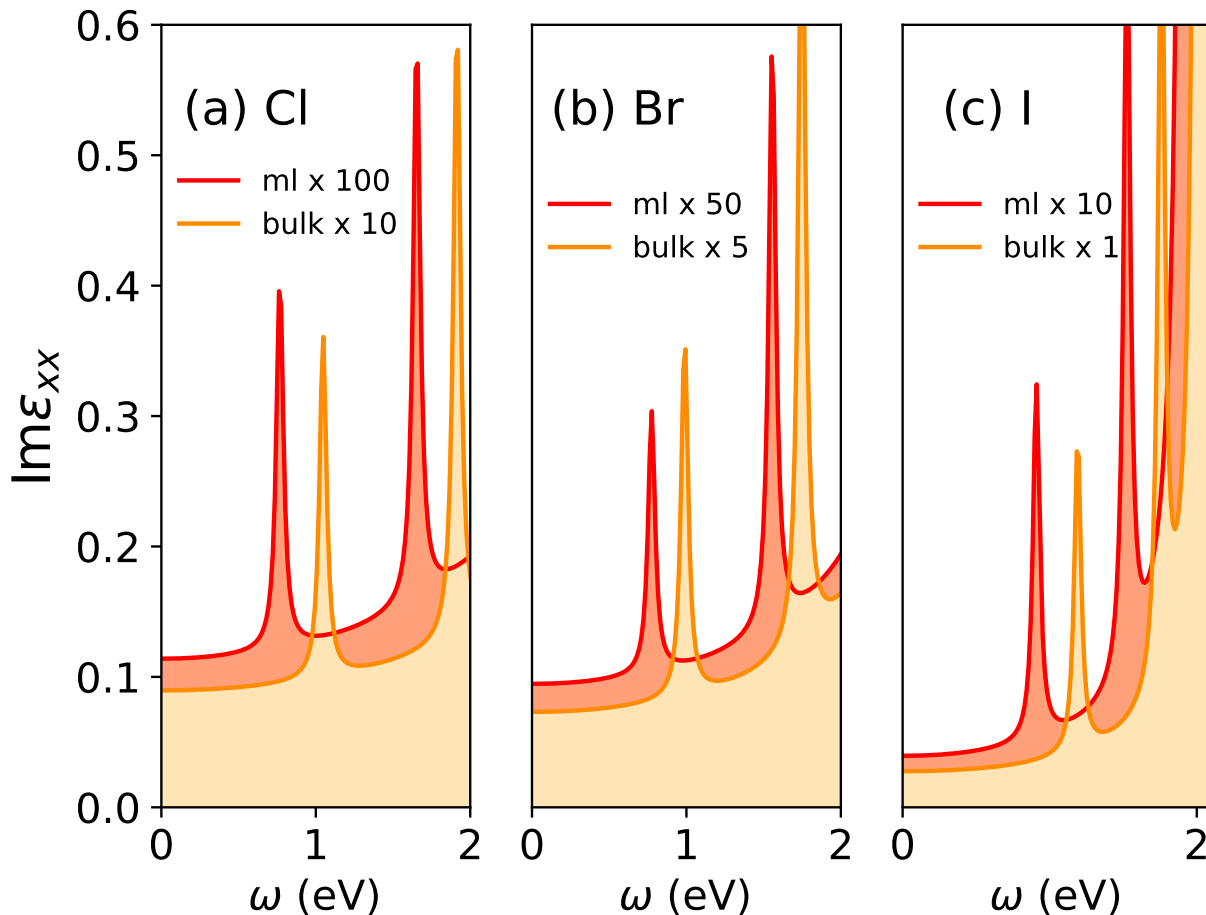


FIG. 2. CrX_3 : The low energy (0 – 2 eV) part of imaginary part of macroscopic dielectric response $\text{Im}\epsilon_{xx}$ with the perturbing electric field applied along the (100) direction of the material, for bulk and free standing monolayers of CrX_3 with (a) $X = \text{Cl}$, (b) $X = \text{Br}$, (c) $X = \text{I}$. Optical broadening of 2 milli-Hartree is used at all energies. The intensities of the peaks are multiplied by some constant factors to bring them to the same scale.

between absorption and PL peaks of Dhillon *et al.* and Zhang *et al.* respectively, is due to the strong electron-lattice coupling. Similar optical absorptions to that of Dillon *et al.* [13] is also confirmed in a recent study on bulk CrBr_3 [39].

Our theoretical results are fully consistent with experimental observations, without the need for spin-orbit coupling, lattice relaxations, or phonons. We find that indeed, the low lying excitons ex_1 and ex_2 are robust in both bulk and monolayer, with modest differences in their position. We note in passing that the present simulations for a free standing monolayer with a 60 Å vacuum, do not precisely correspond to a monolayer on a substrate. The substrate effect is likely to be non-negligible in real systems, since even in the absence of significant covalent bonding to modify the energy band structure, the substrate will increase the dielectric response which should reduce the excitonic binding energy. This could be one reason for the slight overestimate of our predicted binding energy in the ml case. However, later in the paper we discuss the intricate details of the vertex that we consider as one important reason for this overestimation in E_b . While the issue of the ‘exact position’ of such excitons will be discussed in the following sections, clearly, their intensity drops rapidly from bulk to monolayer. Note in Fig. 2 the monolayer intensity is scaled differently to compare against the bulk. This is again fully consistent with experimental observations (see Fig. 1(b) in Zhang *et al.* [11]) and is probably one important reason why in ml- CrX_3 careful PL experiments are needed to pick up these weak exciton intensities, while the conventional absorption or reflection spectroscopy is enough to pick up the excitons in bulk. Nevertheless, our calculations establish that traditional explanations for the origin of these peaks are not needed, but to understand the fundamental nature of these excitons a more careful analysis of the excitonic

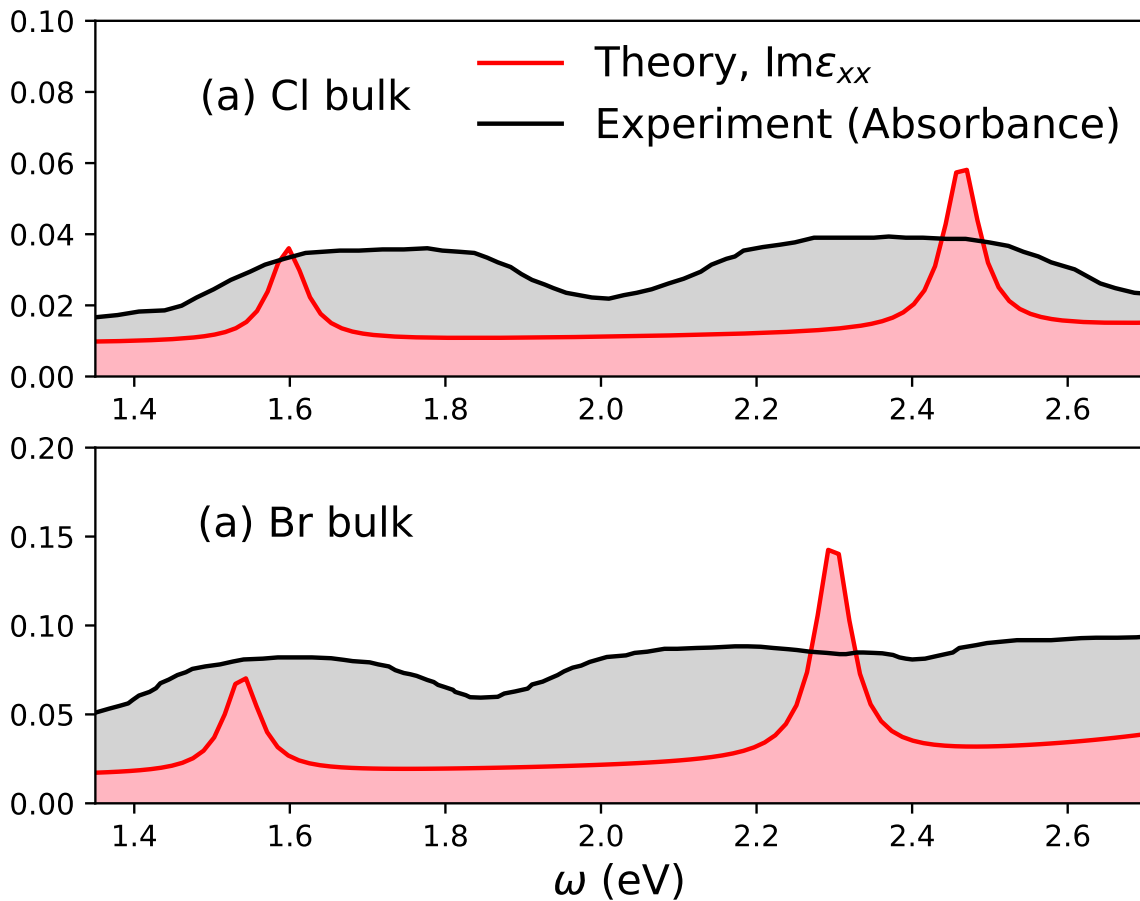


FIG. 3. $\text{CrCl}_3, \text{CrBr}_3$ bulk : Comparison between the adopted optical absorbance data from the recent experimental work on $\text{CrCl}_{3-x}\text{Br}_x$ [39] against our theoretical results. The theoretical spectra for $\text{Im}\epsilon_{xx}$ is rigidly blue-shifted by ~ 0.5 eV as our exciton peaks from $v24c14$ were too deep compared to experiments. Note that need for such manual blue-shifting would not emerge required if we used the dielectric response computed from a smaller two-particle Hamiltonian, say $v12c14$ (see supplemental material).

spectral weights and their origin are required.

Before proceeding, we attempt to benchmark our results for CrI_3 against the existing body of literature. In a recent PL study on ml- CrI_3 [12] an exciton peak is observed at 1.10 eV, and the position hardly changes as the thickness of the sample is increased (see Fig. 4(d) in Seyler *et al.* [12]). From our calculations we also observe the lowest energy exciton ex_1 position at 1.0 eV which is robust across bulk and monolayer variants, much like CrCl_3 and CrBr_3 . We perform a thorough benchmarking of our theoretical optical spectra against what is observed in recent experiments and the agreement is excellent for all energies up to ~ 3.5 eV (see Fig. 4). Also in the study by Seyler *et al.* where the PL intensities are shown for the 1.10 eV peak for bulk, monolayer and layers of different thickness a dramatic drop in the PL intensity can be observed as one goes from bulk to ML limit. This is fully consistent with our calculations [see Fig. 2(c)]: for the same material the $\text{ex}_{1,2}$ peaks can be ~ 10 times more intense in bulk compared to its ML counterpart. Among all these materials the excitons are the most intense in CrI_3 (see Fig. 2). This can be observed also in the old studies on the bulk samples [13, 14]. This is again consistent with our calculations [see Figs. 2(a)-2(c)] where the exciton peaks are the least intense in $\text{X}=\text{Cl}$ and most intense in $\text{X}=\text{I}$. As we show, between ML- CrCl_3 and ML- CrI_3 , the intensity of ex_1 varies by a factor of ~ 10 . This is a signature of the fact that although these two deepest lying excitons in all materials originate fundamentally from transitions between $\text{Cr}-d t_{2g\uparrow}$ and $\text{Cr}-d e_{g\uparrow}$ states, their intensities are directly proportional to the hybridization of the atomic states with the environment. The ($\text{Cr}-d, \text{X}-p$)

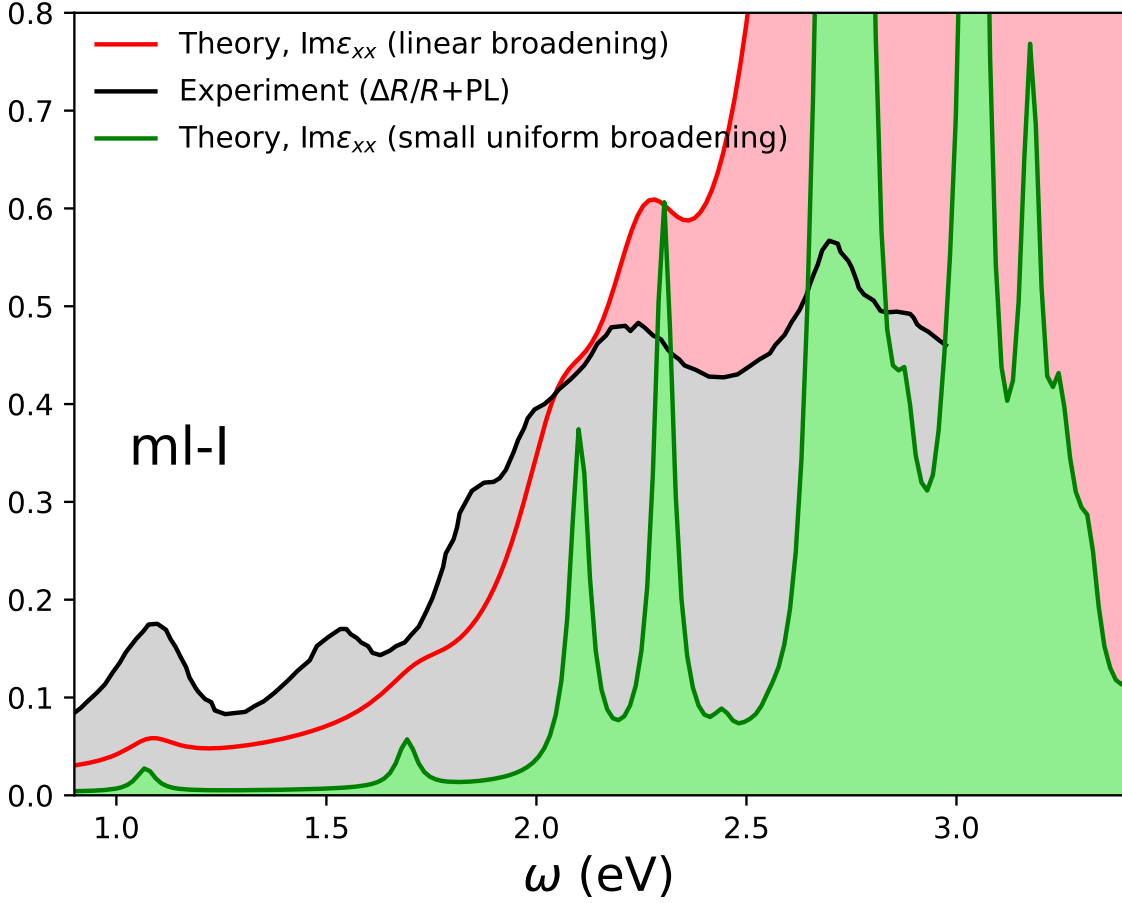


FIG. 4. CrI_3 monolayer : Comparison between the adopted differential reflectivity data combined with low energy photoluminescence data from the recent experimental work on ml- CrI_3 [12] against our theoretical $\text{Im}\epsilon_{xx}$ results. The theoretical spectra for $\text{Im}\epsilon_{xx}$ is rigidly blue-shifted slightly as our exciton peaks from $v24c14$ were by ~ 0.2 eV too deep compared to experiments. The theoretical data for different optical broadening schemes are also plotted on top of the adopted experimental data.

hybridization increases in the sequence $\text{Cl} \rightarrow \text{Br} \rightarrow \text{I}$, and is responsible for the enhancement in the ex_1 intensity leading to brighter excitons. $\text{X}=\text{Cl}$ is the closest to the purely atomic scenario where the hybridization $\text{Cl}-p-\text{Cr}-d$ splitting is largest. To reach an unambiguous conclusion we need to perform further careful analysis of the exciton spectral weights of all these excitons with high-binding energies ($\text{ex}_{1,2,3}$) in the entire class of these bulk and ML magnets. This allows us the opportunity to pin down both their fundamental nature and sensitivity to the ligand states.

We analyze which band pairs and k-points contribute to the $\text{Im}\epsilon_{xx}(\omega)$ exciton spectrum integrated over narrow energy ranges near the peaks of the exciton spectrum. We divide the $\text{QSG}\widehat{W}$ exciton region in separate intervals depending on where the three deepest exciton peaks reside. For example in ML- CrCl_3 the windows would be $[0.6 - 1.4]$, $[1.45 - 2.25]$, and $[2.5 - 3.36]$ eV, corresponding each to a separate peak in the optical spectrum. Fig. 5 shows which band states (n, k) contribute to the exciton eigenvalues. We obtain this figure by using the eigenvectors $|A_{n,k}^\lambda|^2$ of the two-particle Hamiltonian as a weight at each k and band n where λ indicates the exciton eigenvalue and then including all eigenvalues in a given energy range. This is then visualized as the size of the circles on the band structure. The valence bands of primarily of $\text{Cr}-d t_{2g\uparrow}$ characters and conduction bands of primarily $\text{Cr}-d e_{g\uparrow}$ characters contribute to the ex_1 formation in the window $[0.6 - 1.4]$ eV. Intriguingly enough, 10 entire bands ($v6$ and $c4$) contribute almost uniformly (see Fig. 5) across the Brillouin zone to the ex_1 spectral weight. This is true for ex_2 in the window of $[1.45 - 2.25]$ as well, except for parts of the conduction and valence bands (third and fourth conduction bands counted

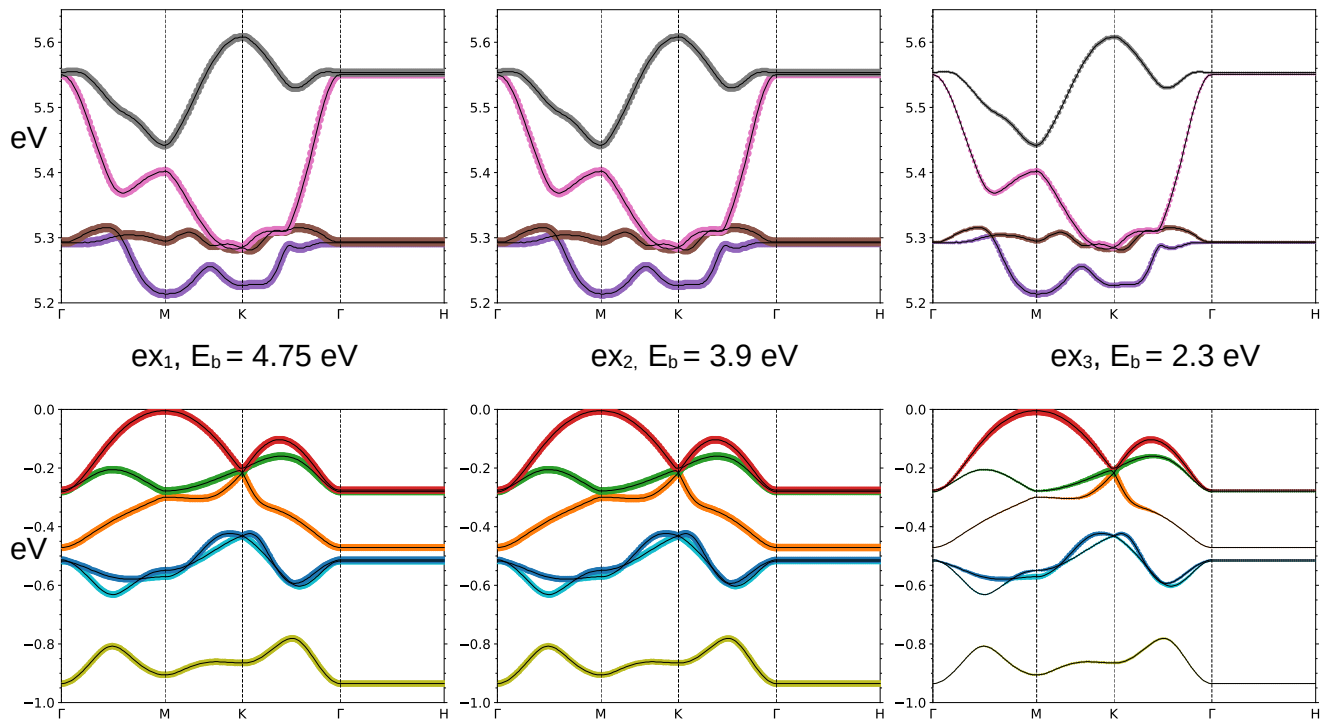


FIG. 5. CrCl₃ Monolayer: The spectral weight analysis for the three deepest lying exciton ex_1 , ex_2 and ex_3 from left to right respectively. The size of the colored circles corresponds to the band contribution to the exciton spectral weight. Almost all the bands containing Cr-3d $t_{2g\uparrow}$ and $e_{g\uparrow}$ orbital characters contribute to $ex_{1,2}$. Exciton spectral weight is almost uniformly spread across these bands in case of $ex_{1,2}$. Spectral weight for ex_3 , which has lesser binding energy compared to $ex_{1,2}$, becomes localized in band basis. Different colors are used to identify different bands.

from the conduction edge, third, forth, fifth and sixth valence bands counted from the valence band top) contribute slightly less compared to other bands. Thus, bands contributing the least to the spectral weight have the most Cl- p character. However, the same analysis for ex_3 shows that mostly the top most valence band and bottom most conduction band contribute to the exciton spectral weight, while the other bands weakly participate in the process. This gives clear indication that in CrCl₃ ex_1 and ex_2 are significantly localized in real space and are of Frenkel nature, while ex_3 is closer to the Wannier-Mott limit. We also note the situation remains invariant whether we perform similar analysis for bulk or ML cases.

Now, we analyze the same across the series Cl \rightarrow Br \rightarrow I. We raise the spectral weight to the fourth power in all cases to identify variations in the band contribution to the spectral weights. We observe that for ex_1 in ML-CrCl₃, while almost all of 6 valence bands and 4 conduction bands contribute uniformly across the BZ, the situation is quite different for the ex_1 in CrI₃. In case of ML-CrI₃, we observe that mostly the two bottom most conduction bands and one top most valence band contribute to ex_1 spectral weight (see Fig. 6), suggesting that the ex_1 in CrI₃ is significantly delocalized in nature compared to the other extreme of CrCl₃. Also, even for the top most valence band, we can identify the red circles becoming larger closer to the M-point and fainter away from that. A careful analysis of the orbital component of this top most valence band shows [27] that the Cr- d orbital character is most prominent at and around M-point while it becomes more I- p like away from it. Altogether, CrI₃ emerges as the extreme case of this series where ex_1 is partially localized in momentum space, in strong contrast to CrCl₃. Similar analysis for both bulk and ML for all cases are performed and the results are shown in the supplemental materials.

To further explore the crucial role of Cr- d -X- p hybridization in determining the intensities and positions of these excitons, we apply a range of weak perturbations to the QSGW two-particle Hamiltonian that modifies the hybridization. Such a physical situation could be simulated within our calculations by either down/up-shifting the X- p centre of mass, down-shifting/up-shifting the Cr- d centre of mass or by adding U to the Cr- d that shifts the Cr majority spin sector down and the minority spin sector up. We try these options on ml-CrBr₃: shift the centre of mass of Br- p up by 0.1 Ry, shift the Cr- d centre of mass down/up by 0.1 Ry and add U=1 eV to Cr- d . We refer to them respectively

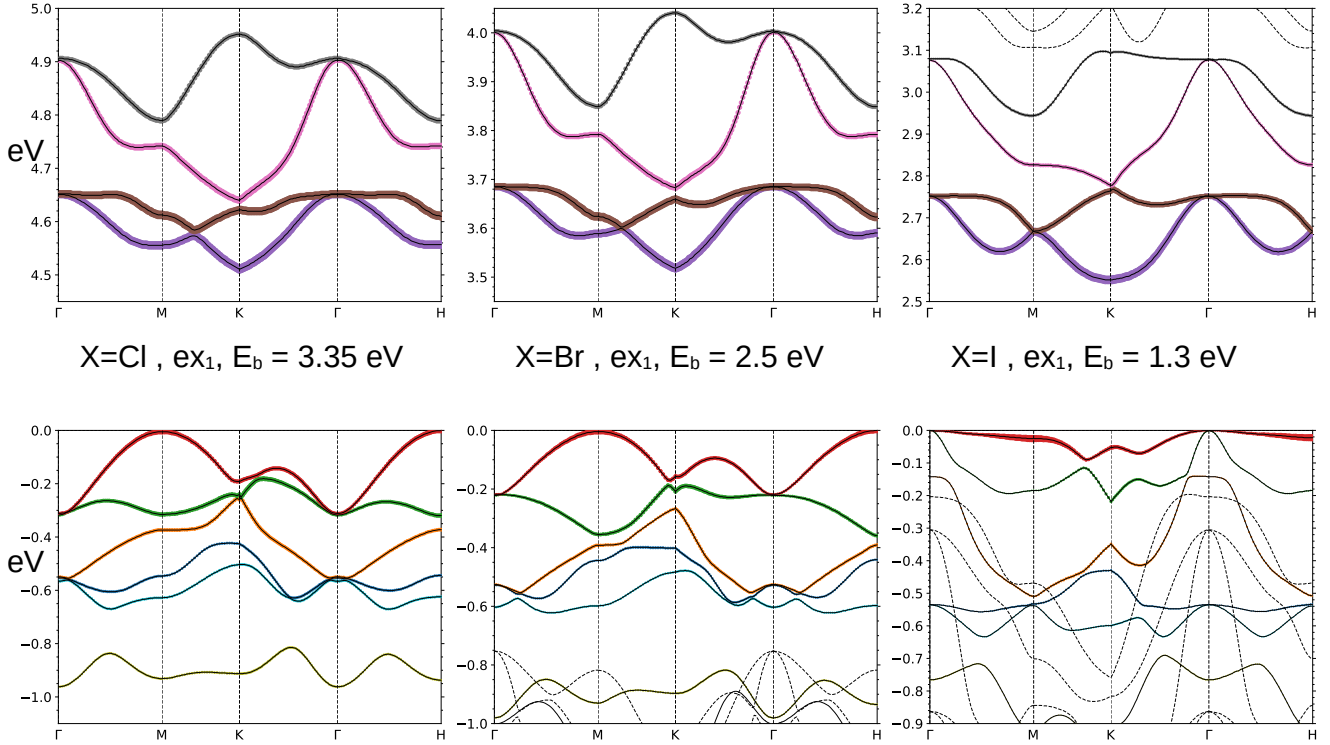


FIG. 6. $\text{CrCl}_3, \text{CrBr}_3, \text{CrI}_3$ bulk : The spectral weight analysis for the deepest lying exciton ex_1 in each case. The spectral weight is raised to the fourth power to identify variations in the band contribution to the spectral weight. In the direction of $\text{Cl} \rightarrow \text{Br} \rightarrow \text{I}$ the number of bands that contribute to the spectral weight of ex_1 decreases. Also the exciton spectral weight becomes more localized in band basis for $\text{X}=\text{I}$, compared to $\text{X}=\text{Cl}, \text{Br}$.

as $Br + 0.1Ry$, $Cr - 0.1Ry$, $Cr + 0.1Ry$ and $Cr, U = 1eV$ for the rest of the discussion. The band gap changes in all cases, so does the hybridization between Cr-d and X-p. For $Cr + 0.1Ry$ (see Fig. 8(e)) the hybridization reduces slightly compared to the original unperturbed case (see Fig. 8(b)) and that leads to less intense exciton peaks (see the blue and black curves in Fig. 8(a)). Also as the atomic nature of the Cr-d becomes more prominent and it reflects in the exciton peaks getting weakly red shifted (larger exciton binding energy E_b) compared to the unperturbed scenario. The reverse happens with $Br + 0.1$ and for $Cr - 0.1Ry$. In both the cases the intensity of the $ex_{1,2}$ peaks increase significantly (see Fig. 8(a) red and purple curves) which is a direct consequence of larger hybridization between Cr-d and Br-p (see Fig. 8(c,d)) while the peak positions also get weakly blue shifted leading to lesser E_b . However, with $Cr, U = 1eV$ the ex_1 gets significantly blue shifted to 1.35 eV (see Fig. 8(a) magenta curve). Note that 1.35 eV is the exact position of the ex_1 from the recent PL study [11] on ml- CrBr_3). In this scenario the valence band manifold becomes dominated by the Br-p (see Fig. 8(f)). This also suggests that the missing details of the Γ , whether it is the dynamics in Γ or the missing Γ itself from the Σ , will most likely lead to the same qualitative effect leading to the correction in the absolute positions of these deep lying excitons. Within our \widehat{QSGW} framework, vertex is explicitly included in W and is absent from Σ . One primary effect of including Γ in Σ is to modify the relative centre of masses of Cr-d and X-p. Note that our E_{ex_1} estimation was ~ 0.5 eV off (too deep) in both bulk and ml. With $Cr, U = 1eV$ we can correct E_{ex_1} by ~ 0.5 eV in both bulk and ml. Hence, the discrepancy between our theory and experiment is related to the exact nature of the vertex and not the dimensionality of the material. This is also intuitive that this discrepancy is large (~ 0.5 eV) in $\text{X}=\text{Cl}, \text{Br}$ where the systems are most atomic in nature and smaller (~ 0.2 eV) in $\text{X}=\text{I}$, where it is least atomic or most band-like. It is expected that the dynamics in vertex or a better vertex altogether (possibly from approaches that are more 'exact' than these many body perturbative approaches) is more relevant in the atomic scenario.

To further verify the Frenkel-ness of the excitons, we apply moderate volume conserving strain ϵ on the monolayers of CrBr_3 and CrI_3 . We observe that the positions of the excitons $ex_{1,2}$, E_{ex} remain invariant with both tensile and compressive strains in $\text{X}=\text{Br}$ while it changes in $\text{X}=\text{I}$ by roughly 100 meV for compressive strain $\epsilon = 7\%$. Weak changes with tensile ϵ in $\text{X}=\text{I}$ can also be observed. This is consistent with our conclusions of excitons being most

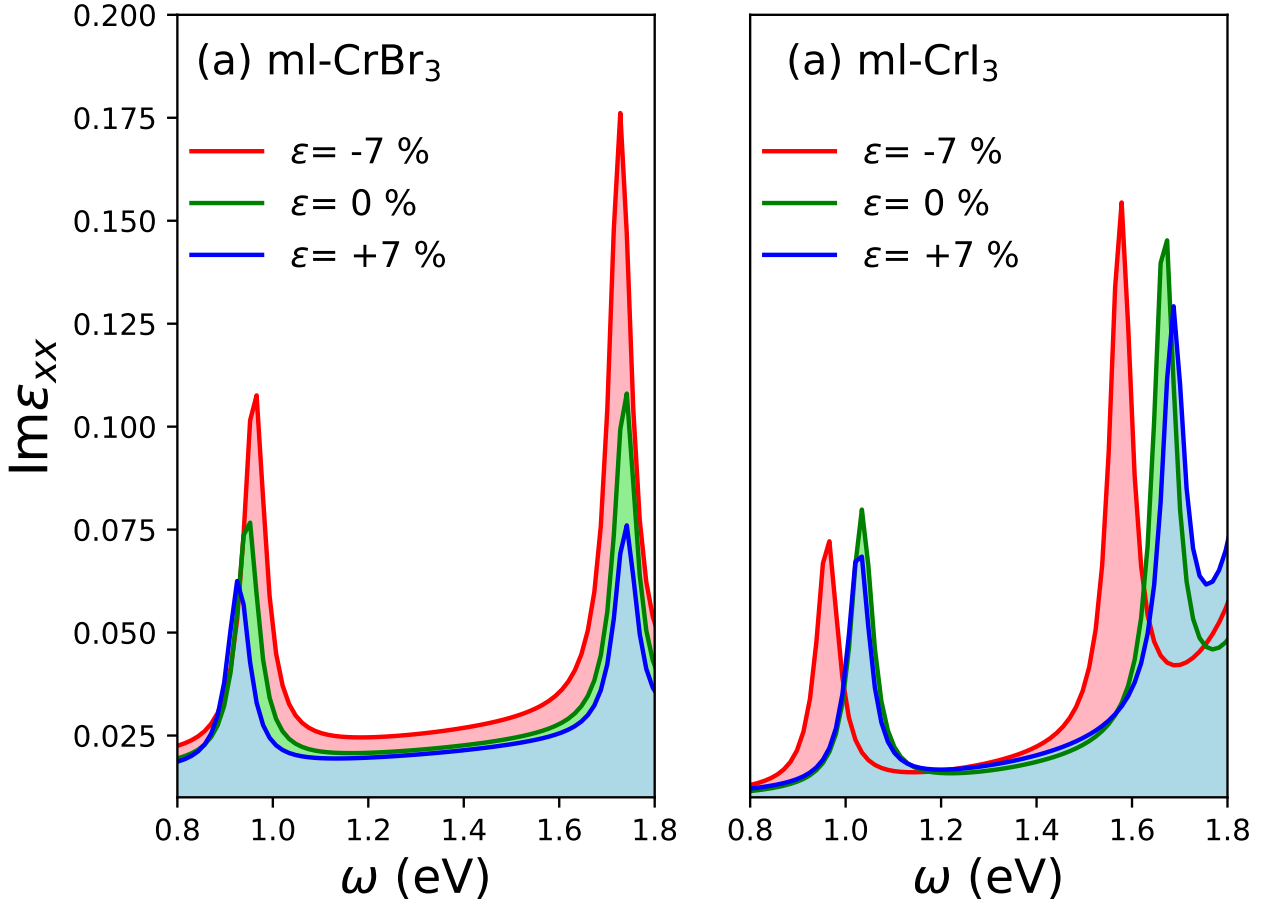


FIG. 7. CrBr₃, CrI₃ Monolayer : Volume conserving tensile and compressive strains ϵ are applied. E_{ex} does not change for X=Br, while it changes by 100 meV for compressive strain of $\epsilon=7\%$ in X=I. Intensities of the peaks are multiplied by a constant factor of three in ml-CrBr₃ to bring them to the same scale as ml-CrI₃.

Frenkel like in X=Cl,Br and more Wannier-Mott like in X=I.

While what we should characterize as a proper Frenkel exciton is a matter of definition, it becomes apparent from our analysis that even for the deepest lying exciton with the largest binding energy, it is most Frenkel like in CrCl₃ and the least Frenkel like in CrI₃. We show that the lighter the halogen is, the weaker is the intensity of these Frenkel excitons making it even more challenging experimentally to observe them. Nevertheless, for a given material, as we look for excitons with lesser binding energies, for example ex₃, in all cases, is the closest analogue of Wannier-Mott exciton, in the sense of what is observed in, say, LiF or MoS₂. The degree of ‘Wannier-Mott’-ness is proportional to the degree of hybridization between the Cr-*d* and X-*p* states, thereby supporting *the picture* of a ‘band-origin’ for these excitons in CrX₃. The band-origin also suggests that it is, probably, possible to tweak their binding energies and intensities by applying shear, strain, magnetic field or simply by scanning across the periodic table looking for elements with varying degree of hybridization. However, as we show tensile or compressive strains lead to no (in X=Cl,Br) or weak changes (in X=I) to the exciton positions, suggesting that effectively these deep lying excitons across this entire class of systems are mostly Frenkel like. One interesting aspect would be to realize crystals made of Cr and F, and/or Cr and O in the same crystalline space-group as the rest.

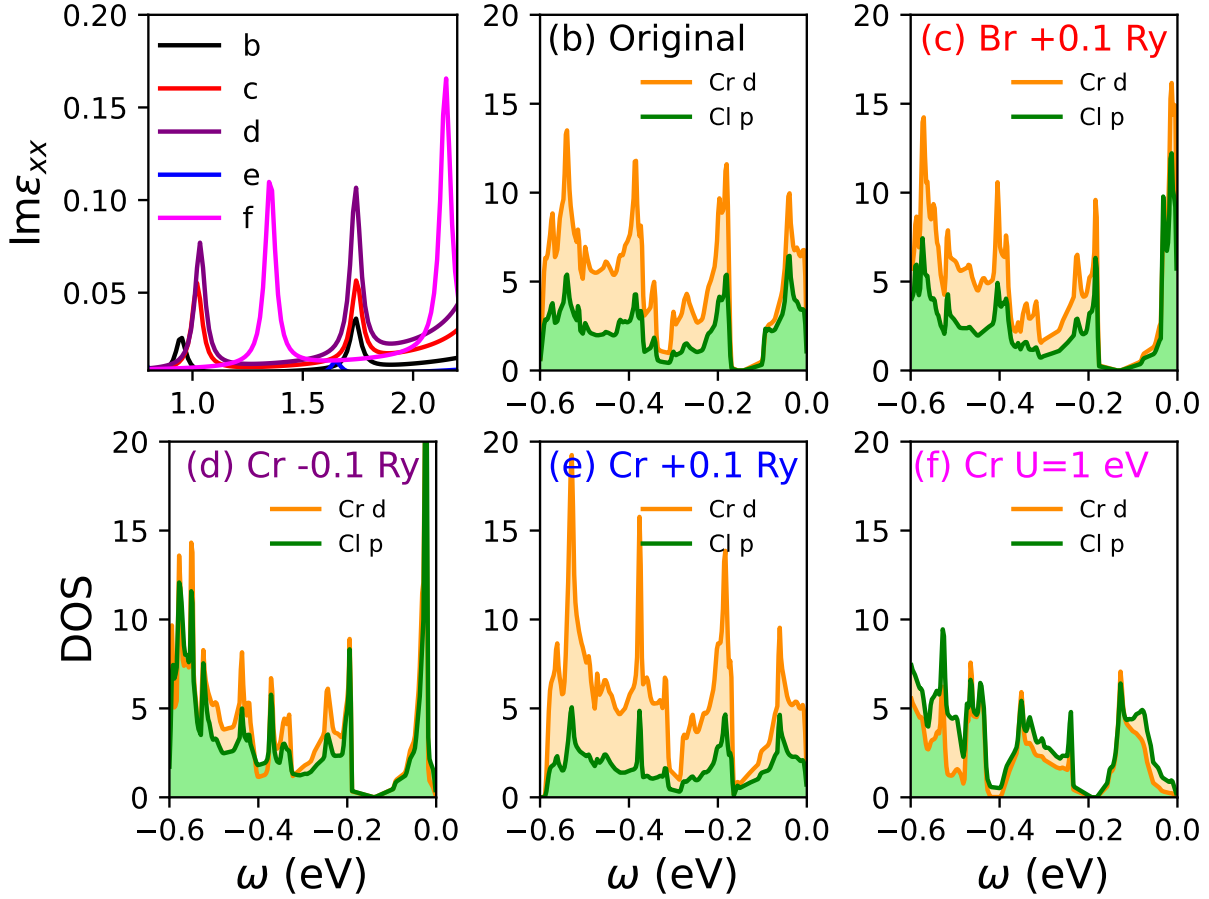


FIG. 8. CrBr₃ Monolayer: QSGW results in different circumstances. $Br + 0.1Ry$ shifts the Br-p centre of mass up by 0.1 Ry, $Cr - 0.1Ry$ and $Cr + 0.1Ry$ down/up shifts Cr-d the centre of mass by 0.1 Ry and $CrU = 1eV$ adds $U=1$ eV Cr-d. In cases with larger Cr-d and Br-p hybridization the excitons become more intense and get blue shifted and the reverse happens for lesser hybridization. However, the position of $ex_{1,2}$ changes dramatically for $CrU = 1eV$.

CONCLUSIONS

Our work summarily excludes the stringent requirement of relaxation of the Laporte Rule, that forbids the ‘atomic’ $d-d$ transitions based on symmetry arguments, as a fundamental principle of origin of these excitons in CrX₃. While the deepest lying excitons are mostly localized on the Cr-d orbitals, they delocalize within the unit cell on the X-p orbitals as well. The degree of delocalization and real-space range of these excitons increase as the halogen atoms become heavier and contains more core states that are shallower compared to the Cr-d states. This suggests, if CrF₃ exists that could host the most localized Frenkel-like excitons, with the largest binding energies, from the entire series with, probably, the closest analogue of what can be characterized as purely atomic $d-d$ transition. Nevertheless, in real world and crystalline environment there should always exist finite, albeit small, hybridization between different angular momentum states, leading to invariably ‘band-origin’ of excitons in all cases. We explicitly show that it is possible to modify both the intensities and positions of these excitons by applying weak perturbation to the Hamiltonian that changes the hybridization environment.

ACKNOWLEDGEMENTS

MIK, ANR and SA are supported by the ERC Synergy Grant, project 854843 FASTCORR (Ultrafast dynamics of correlated electrons in solids). This work was authored (in part) by the National Renewable Energy Laboratory, operated by Alliance for Sustainable Energy, LLC, for the U.S. Department of Energy (DOE) under Contract No. DE-AC36-08GO28308. Funding was provided by the Theoretical Condensed Matter Physics program within the Office of Basic Energy Sciences. The views expressed in the article do not necessarily represent the views of the DOE or the U.S. Government. The U.S. Government retains and the publisher, by accepting the article for publication, acknowledges that the U.S. Government retains a nonexclusive, paid-up, irrevocable, worldwide license to publish or reproduce the published form of this work, or allow others to do so, for U.S. Government purposes. We acknowledge PRACE for awarding us access to Irene-Rome hosted by TGCC, France and Juwels Booster and Cluster, Germany.

METHOD

Single particle calculations (DFT, and energy band calculations with the static quasiparticlized $QSGW$ self-energy $\Sigma^0(k)$) were performed on a $12 \times 12 \times 1$ k -mesh while the (relatively smooth) dynamical self-energy $\Sigma(k)$ was constructed using a $6 \times 6 \times 1$ k -mesh and $\Sigma^0(k)$ extracted from it. For each iteration in the $QSGW$ self-consistency cycle, the charge density was made self-consistent. The $QSGW$ cycle was iterated until the RMS change in Σ^0 reached 10^{-5} Ry. Thus the calculation was self-consistent in both $\Sigma^0(k)$ and the density. Numerous checks were made to verify that the self-consistent $\Sigma^0(k)$ was independent of starting point, for both $QSGW$ and $QSG\widehat{W}$ calculations; e.g. using LDA or Hartee-Fock self-energy as the initial self energy for $QSGW$ and using LDA or $QSGW$ as the initial self-energy for $QSG\widehat{W}$. We achieve these optical spectra in Fig. 2 using a uniform optical broadening of 2 milli-Hartree at all energies, so that the peaks can be identified clearly. By contrast, in Fig. 1 an energy-dependent broadening that linearly varies from 2 milli-Hartree at the lowest energies to maximum of 50 milli-Hartree at the highest energy (at 1 Rydberg) was used.

COMPETING INTERESTS

The authors declare no competing financial or non-financial interests.

CORRESPONDENCE

All correspondence, code and data requests should be made to SA.

DATA AVAILABILITY

All input/output data can be made available on reasonable request. All the input file structures and the commandlines to launch calculations are rigorously explained in the tutorials available on the Questaal webpage [40].

CODE AVAILABILITY

The source codes for LDA, $QSGW$ and $QSG\widehat{W}$ are available from [40] under the terms of the AGPLv3 license.

SUPPLEMENTAL MATERIAL

In the supplemental material we benchmark our results with previous theoretical and experimental results, perform the spectral weight analysis for the excitons in bulk and monolayer variants and convergence in E_{ex} with varying two-particle Hamiltonian sizes.

Benchmarking against existing theoretical and experimental results:

The recent work by Wu *et al.* [29] predicts $E_b=2.3$ eV in monolayer CrBr₃ for the deepest lying bright exciton. From their one shot L(S)DA+ GW calculations they achieve $E_g = 3.8$ eV. However, when they solve the GW +BSE to find the deepest lying bright exciton ex_1 , the peak is observed at $E_{ex} = 1.5$ eV, thereby leading to $E_b = 2.3$ eV. Note that our estimation of $E_b = 2.5$ eV from bulk-CrBr₃ is very similar to their estimation, nevertheless, our estimation of $E_b = 3.85$ eV from ml-CrBr₃ is much higher. The primary reason for this originates from the difference in the one-particle gap (4.65 eV in QSGW compared to 3.8 eV from DFT+ U + GW). Also, the two-particle Hamiltonian that we solve within QSGW contains 24 valence and 14 conduction states, leading to $E_{ex} = 0.8$ eV. As we show below, a modestly different E_{ex} is obtained when we use 21(v)+14(c) as Wu *et al.* did. The absolute position of E_{ex} is much slower to converge than the relative splittings of the two bright excitons, as we show below. This can be simply understood in terms of the orbitals contributing to the excitons: the highest valence bands contain the 6 Cr-3d- $t_{2g\uparrow}$ states and 18 X- p states (the unit cell contains 2 Cr atoms and 6 X atoms). These hybridize and all of them contribute to the exciton. Wu *et al.* [29] argues that unlike monolayer transition metal dichalcogenides where the lowest-energy bright excitons are of Wannier type with a diameter of several nanometers [41, 42], ML-CrBr₃ hosts bright charge-transfer exciton states that extend over a few primitive cells, indicating formation of band transitions instead of intra-atomic $d-d$ transitions. They further argue that exciton distribution in ML-CrBr₃ is consistent with the intuition that a larger exciton binding energy is associated with a smaller exciton radius [43]. Their findings for ML-CrBr₃ are consistent with our present observations, and indeed they extend to the entire CrX₃ (X=Cl,Br,I) family, both ML and bulk.

Further, we benchmark our results against the study by Molina *et al.* [28] who uses a very similar method like Wu *et al.* [29], namely, L(S)DA+ GW . Also in both the works [28, 29] the choice of the L(S)DA eigenfunctions as starting eigenfunctions for their single-shot GW calculations is completely consistent as both uses $U = 1.5$ eV and $J = 0.5$ eV. Molina *et al.* [28] achieves $E_g = 4.45$ eV for ml-CrBr₃ and $E_{ex} = 2.40$ eV, leading to $E_b = 2.05$ eV. The fact that the E_{ex} , in this study by Molina *et al.*, is significantly blue shifted (~ 1 eV compared to Wu *et al.* [29] and ~ 1.6 eV compared to our work) could be due to many reasons, the primary of which we think is the incomplete convergence in the two-particle Hamiltonian size. However, we could not find any comment in these two works about the convergence check in terms of the vacuum size. As we showed in our previous work [27] the vacuum correction, further, can lead to enhancement in E_g in ml-CrBr₃ by ~ 0.4 eV, and hence, could be a natural explanation for an enhanced estimation of E_b in our work.

* swagata.acharya@ru.nl

- [1] G. H. Wannier, "The structure of electronic excitation levels in insulating crystals," *Phys. Rev.*, vol. 52, pp. 191–197, Aug 1937.
- [2] D. Y. Qiu, H. Felipe, and S. G. Louie, "Optical spectrum of mos 2: many-body effects and diversity of exciton states," *Physical review letters*, vol. 111, no. 21, p. 216805, 2013.
- [3] Z. Ye, T. Cao, K. O'Brien, H. Zhu, X. Yin, Y. Wang, S. G. Louie, and X. Zhang, "Probing excitonic dark states in single-layer tungsten disulphide," *Nature*, vol. 513, no. 7517, pp. 214–218, 2014.
- [4] S. K. Radha, W. R. Lambrecht, B. Cunningham, M. Grüning, D. Pashov, and M. van Schilfhaarde, "Optical response and band structure of licoo2 including electron-hole interaction effects," *arXiv preprint arXiv:2106.09137*, 2021.
- [5] J. Frenkel, "On the transformation of light into heat in solids. i," *Phys. Rev.*, vol. 37, pp. 17–44, Jan 1931.
- [6] J. Frenkel, "On the transformation of light into heat in solids. ii," *Phys. Rev.*, vol. 37, pp. 1276–1294, May 1931.
- [7] V. Agranovich and B. Tshich, "Collective properties of frenkel excitons," *Sov. Phys. JETP*, vol. 26, no. 1, pp. 104–112, 1968.
- [8] E. E. Jelley, "Spectral absorption and fluorescence of dyes in the molecular state," *Nature*, vol. 138, no. 3502, pp. 1009–1010, 1936.
- [9] T. Nematiram, D. Padula, and A. Troisi, "Bright frenkel excitons in molecular crystals: A survey," *Chemistry of Materials*, vol. 33, no. 9, pp. 3368–3378, 2021.
- [10] B. A. West, J. M. Womick, L. McNeil, K. J. Tan, and A. M. Moran, "Ultrafast dynamics of frenkel excitons in tetracene and rubrene single crystals," *The Journal of Physical Chemistry C*, vol. 114, no. 23, pp. 10580–10591, 2010.
- [11] Z. Zhang, J. Shang, C. Jiang, A. Rasmita, W. Gao, and T. Yu, "Direct photoluminescence probing of ferromagnetism in monolayer two-dimensional crbr3," *Nano Lett.*, vol. 19, no. 5, pp. 3138–3142, 2019.
- [12] K. L. Seyler, D. Zhong, D. R. Klein, S. Gao, X. Zhang, B. Huang, E. Navarro-Moratalla, L. Yang, D. H. Cobden, M. A. McGuire, *et al.*, "Ligand-field helical luminescence in a 2d ferromagnetic insulator," *Nature Physics*, vol. 14, no. 3, pp. 277–281, 2018.
- [13] J. Dillon Jr, H. Kamimura, and J. Remeika, "Magneto-optical properties of ferromagnetic chromium trihalides," *Journal*

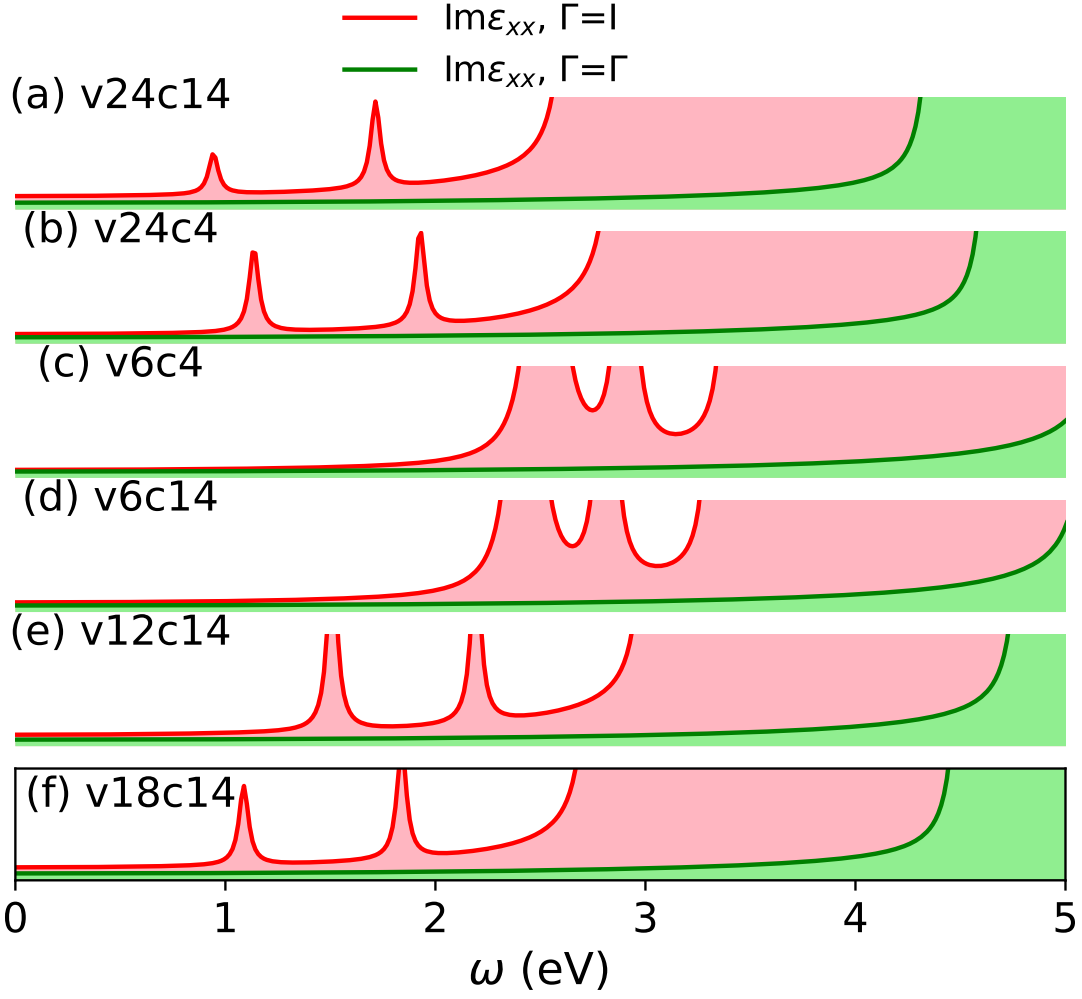


FIG. 9. CrBr₃ Monolayer: Convergence in E_{ex} with the two-particle Hamiltonian size by varying the numbers of valence (v) and conduction bands (c). The green curves that are for the RPA- $\text{Im}\epsilon_{xx}$ (the vertex Γ put to I) also changes for different v - c choices, since the one-particle eigenfunctions change in each case. The exciton peaks and the optical spectral weight gets redshifted with larger v - c choices, as more screening channels are included. The E_{ex} is most sensitive to v and weakly depends on c for $c \geq 4$ (the critical number of bands that contain mostly the Cr- d - $e_{g\uparrow}$ states).

of *Physics and Chemistry of Solids*, vol. 27, no. 9, pp. 1531–1549, 1966.

- [14] P. Grant and G. Street, “Optical properties of chromium trihalides in region 1-11 ev,” in *Bulletin of the American Physical Society*, vol. 13, p. 415, AMER INST PHYSICS CIRCULATION FULFILLMENT DIV, 500 SUNNYSIDE BLVD, WOODBURY . . . , 1968.
- [15] I. Pollini and G. Spinolo, “Intrinsic optical properties of crcl₃,” *physica status solidi (b)*, vol. 41, no. 2, pp. 691–701, 1970.
- [16] V. M. Bermudez and D. S. McClure, “Spectroscopic studies of the two-dimensional magnetic insulators chromium trichloride and chromium tribromide—i,” *Journal of Physics and Chemistry of Solids*, vol. 40, no. 2, pp. 129–147, 1979.
- [17] L. Nosenzo, G. Samoggia, and I. Pollini, “Effect of magnetic ordering on the optical properties of transition-metal halides: Ni cl 2, ni br 2, cr cl 3, and cr br 3,” *Physical Review B*, vol. 29, no. 6, p. 3607, 1984.
- [18] B. Huang, G. Clark, E. Navarro-Moratalla, D. R. Klein, R. Cheng, K. L. Seyler, D. Zhong, E. Schmidgall, M. A. McGuire, D. H. Cobden, *et al.*, “Layer-dependent ferromagnetism in a van der waals crystal down to the monolayer limit,” *Nature*, vol. 546, no. 7657, pp. 270–273, 2017.
- [19] D. R. Klein, D. MacNeill, J. L. Lado, D. Soriano, E. Navarro-Moratalla, K. Watanabe, T. Taniguchi, S. Manni, P. Canfield, J. Fernández-Rossier, *et al.*, “Probing magnetism in 2d van der waals crystalline insulators via electron tunneling,” *Science*, vol. 360, no. 6394, pp. 1218–1222, 2018.
- [20] M. Kim, P. Kumaravadeivel, J. Birkbeck, W. Kuang, S. G. Xu, D. Hopkinson, J. Knolle, P. A. McClarty, A. Berdyugin, M. B. Shalom, *et al.*, “Micromagnetometry of two-dimensional ferromagnets,” *Nature Electronics*, vol. 2, no. 10, pp. 457–463, 2019.

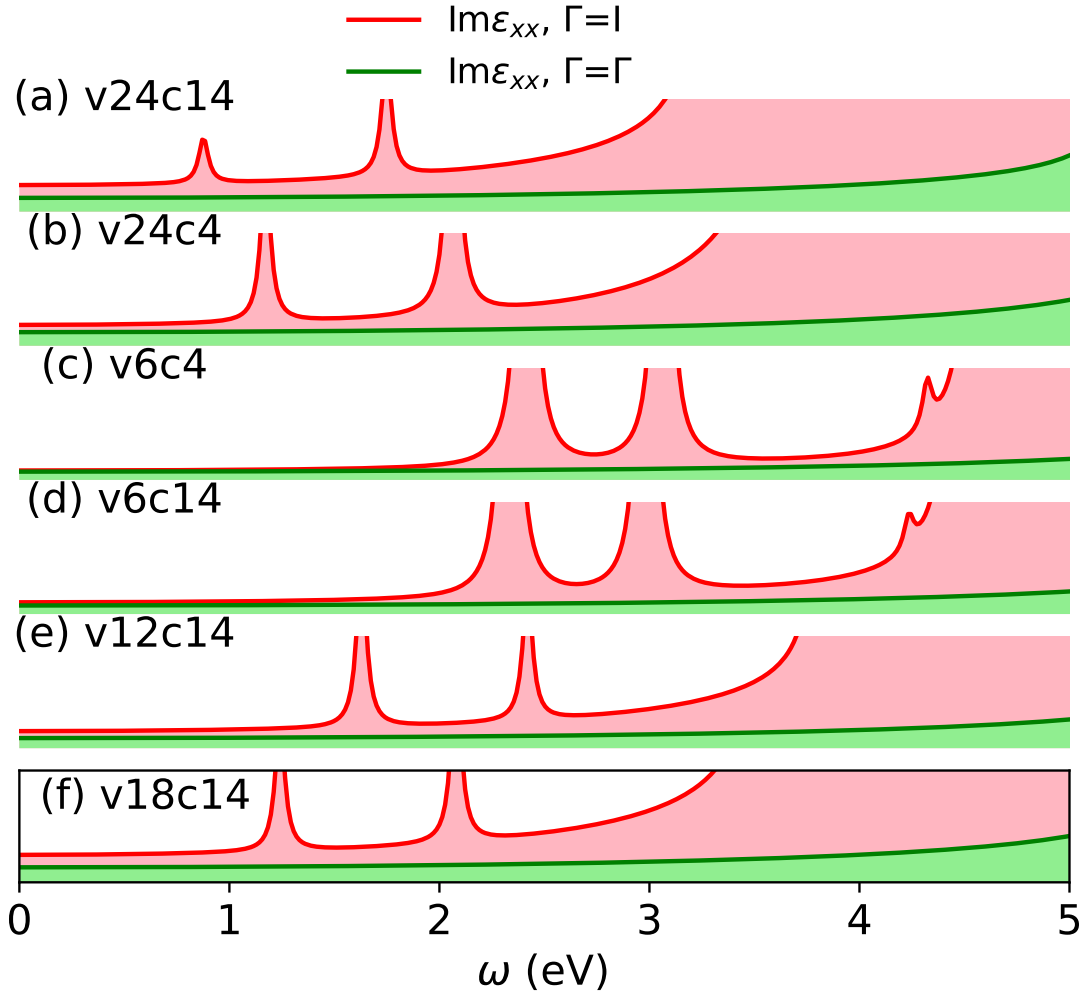


FIG. 10. CrCl₃ Monolayer: Coverage in E_{ex} with the two-particle Hamiltonian size by varying the numbers of valence (v) and conduction bands (c). The green curves that are for the RPA- $\text{Im}\epsilon_{xx}$ (the vertex Γ put to I) also changes for different vc choices, since the one-particle eigenfunctions change in each case. The exciton peaks and the optical spectral weight gets redshifted with larger v - c choices, as more screening channels are included. The E_{ex} is most sensitive to v and weakly depends on c for $c \geq 4$ (the critical number of bands that contain mostly the Cr- d - $e_{g\uparrow}$ states).

- [21] X. Cai, T. Song, N. P. Wilson, G. Clark, M. He, X. Zhang, T. Taniguchi, K. Watanabe, W. Yao, D. Xiao, *et al.*, “Atomically thin crcl3: an in-plane layered antiferromagnetic insulator,” *Nano letters*, vol. 19, no. 6, pp. 3993–3998, 2019.
- [22] C. Gong, L. Li, Z. Li, H. Ji, A. Stern, Y. Xia, T. Cao, W. Bao, C. Wang, Y. Wang, *et al.*, “Discovery of intrinsic ferromagnetism in two-dimensional van der waals crystals,” *Nature*, vol. 546, no. 7657, pp. 265–269, 2017.
- [23] Z. Fei, B. Huang, P. Malinowski, W. Wang, T. Song, J. Sanchez, W. Yao, D. Xiao, X. Zhu, A. F. May, *et al.*, “Two-dimensional itinerant ferromagnetism in atomically thin fe 3 gete 2,” *Nature materials*, vol. 17, no. 9, pp. 778–782, 2018.
- [24] Y. Deng, Y. Yu, M. Z. Shi, Z. Guo, Z. Xu, J. Wang, X. H. Chen, and Y. Zhang, “Quantum anomalous hall effect in intrinsic magnetic topological insulator mmbi2te4,” *Science*, vol. 367, no. 6480, pp. 895–900, 2020.
- [25] C. Gong and X. Zhang, “Two-dimensional magnetic crystals and emergent heterostructure devices,” *Science*, vol. 363, no. 6428, 2019.
- [26] M. Gibertini, M. Koperski, A. Morpurgo, and K. Novoselov, “Magnetic 2d materials and heterostructures,” *Nature nanotechnology*, vol. 14, no. 5, pp. 408–419, 2019.
- [27] S. Acharya, D. Pashov, B. Cunningham, A. N. Rudenko, M. Rösner, M. Grüning, M. van Schilfhaarde, and M. I. Katsnelson, “Electronic structure of chromium trihalides beyond density functional theory,” *Phys. Rev. B*, vol. 104, p. 155109, Oct 2021.
- [28] A. Molina-Sánchez, G. Catarina, D. Sangalli, and J. Fernández-Rossier, “Magneto-optical response of chromium trihalide monolayers: chemical trends,” *J. Mater. Chem. C*, vol. 8, no. 26, pp. 8856–8863, 2020.
- [29] M. Wu, Z. Li, and S. G. Louie, “Optical and magneto-optical properties of ferromagnetic monolayer crbr₃: A first-principles

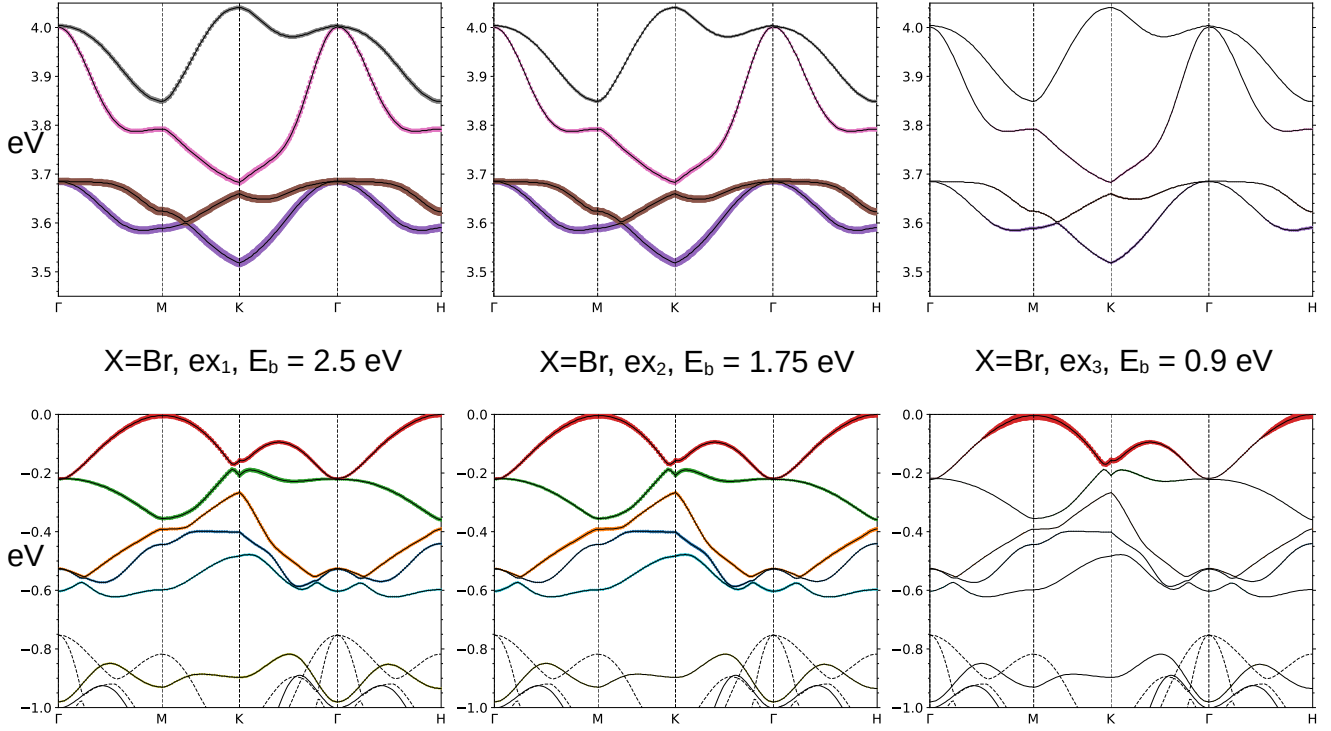


FIG. 11. CrBr_3 bulk : The spectral weight analysis for the three deepest lying exciton ex_1 , ex_2 and ex_3 from left to right respectively. Almost all the bands containing $\text{Cr-}3d$ $t_{2g\uparrow}$ and $e_{g\uparrow}$ orbital characters contribute to $\text{ex}_{1,2}$. Exciton spectral weight is almost uniformly spread across these bands in case of $\text{ex}_{1,2}$. Spectral weight for ex_3 , which has lesser binding energy compared to $\text{ex}_{1,2}$, becomes localized in band basis.

gw and *gw* plus bethe-salpeter equation study,” 2021.

- [30] M. van Schilfgaarde, T. Kotani, and S. Faleev, “Quasiparticle Self-Consistent *GW* Theory,” *Phys. Rev. Lett.*, vol. 96, no. 22, p. 226402, 2006.
- [31] T. Kotani, M. van Schilfgaarde, and S. V. Faleev, “Quasiparticle self-consistent *GW* method: A basis for the independent-particle approximation,” *Phys. Rev. B*, vol. 76, p. 165106, 2007.
- [32] D. Pashov, S. Acharya, W. R. L. Lambrecht, J. Jackson, K. D. Belashchenko, A. Chantis, F. Jamet, and M. van Schilfgaarde, “Questaal: a package of electronic structure methods based on the linear muffin-tin orbital technique,” *Comp. Phys. Comm.*, vol. 249, p. 107065, 2020.
- [33] S. Ismail-Beigi, “Justifying quasiparticle self-consistent schemes via gradient optimization in Baym–Kadanoff theory,” *J. Phys.: Condens. Matter*, vol. 29, p. 385501, 2017.
- [34] B. Cunningham, M. Gruening, D. Pashov, and M. van Schilfgaarde, “QSGW: Quasiparticle Self consistent GW with ladder diagrams in W.” Preprint arXiv 2106.05759, 2021.
- [35] B. Cunningham, M. Grüning, P. Azarhoosh, D. Pashov, and M. van Schilfgaarde, “Effect of ladder diagrams on optical absorption spectra in a quasiparticle self-consistent GW framework,” *Phys. Rev. Mater.*, vol. 2, p. 034603, 2018.
- [36] S. Hirata and M. Head-Gordon, “Time-dependent density functional theory within the tamm–dancoff approximation,” *Chemical Physics Letters*, vol. 314, no. 3-4, pp. 291–299, 1999.
- [37] G. Myrta, A. Marini, and X. Gonze, “Exciton-plasmon states in nanoscale materials breakdown of the tamm–dancoff approximation,” *Nano Letters*, vol. 9, no. 8, pp. 2820–2824, 2009.
- [38] S. Acharya, D. Pashov, A. N. Rudenko, M. Rösner, M. van Schilfgaarde, and M. I. Katsnelson, “First principles vs second principles: Role of charge self-consistency in strongly correlated systems,” *arXiv preprint arXiv:2106.12090*, 2021.
- [39] M. Abramchuk, S. Jaszewski, K. R. Metz, G. B. Osterhoudt, Y. Wang, K. S. Burch, and F. Tafti, “Controlling magnetic and optical properties of the van der waals crystal crcl_3 - xbrx via mixed halide chemistry,” *Advanced Materials*, vol. 30, no. 25, p. 1801325, 2018.
- [40] <https://www.questaal.org>. Questaal code website.
- [41] Z. Ye, T. Cao, K. O’Brien, H. Zhu, X. Yin, Y. Wang, S. G. Louie, and X. Zhang, “Probing excitonic dark states in single-layer tungsten disulphide,” *Nature*, vol. 513, no. 7517, pp. 214–218, 2014.
- [42] D. Y. Qiu, F. H. da Jornada, and S. G. Louie, “Optical spectrum of mos_2 : Many-body effects and diversity of exciton states,” *Phys. Rev. Lett.*, vol. 111, p. 216805, Nov 2013.

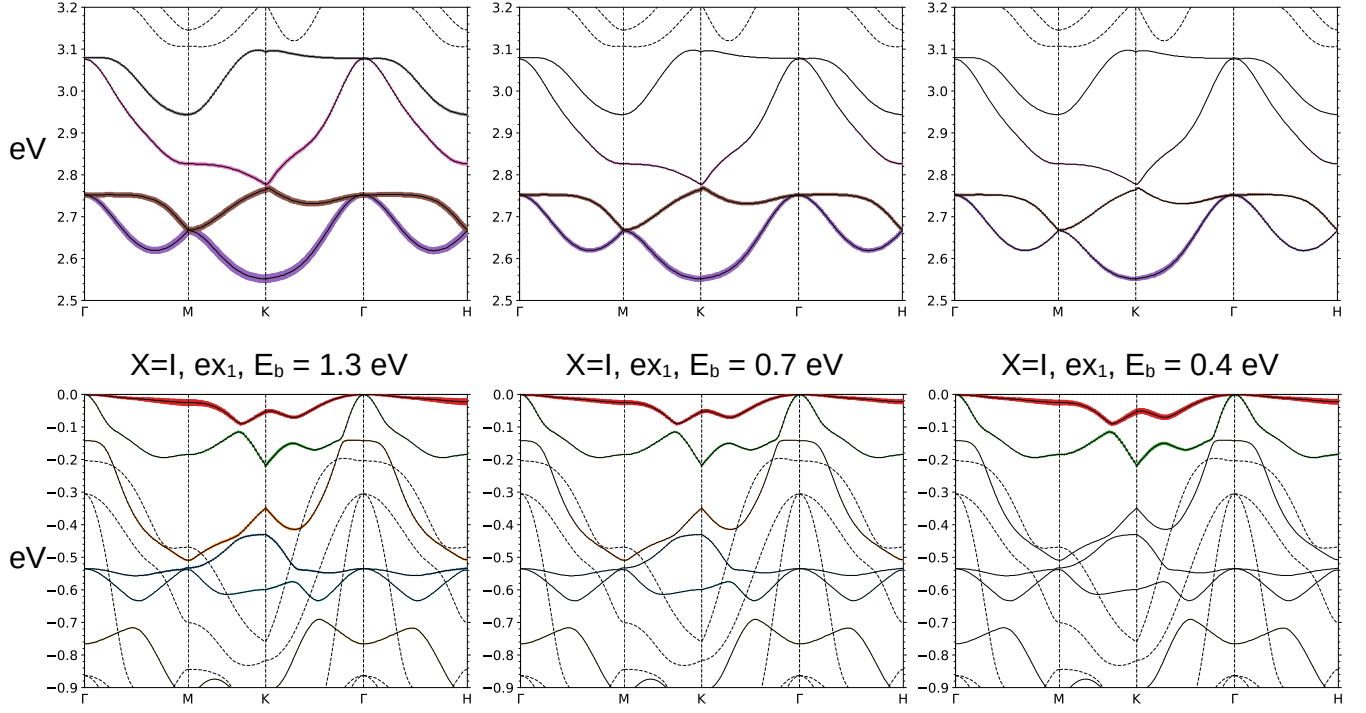


FIG. 12. CrI_3 bulk : The spectral weight analysis for the three deepest lying exciton ex_1 , ex_2 and ex_3 from left to right respectively. Almost all the bands containing Cr-3d $t_{2g\uparrow}$ and $e_{g\uparrow}$ orbital characters contribute to $\text{ex}_{1,2}$. Exciton spectral weight is almost uniformly spread across these bands in case of $\text{ex}_{1,2}$. Spectral weight for ex_3 , which has lesser binding energy compared to $\text{ex}_{1,2}$, becomes localized in band basis.

[43] M. L. Cohen and S. G. Louie, *Fundamentals of condensed matter physics*. Cambridge University Press, 2016.